Interaction and Multiscale Mechanics, Vol. 1, No. 4 (2008) 411-422
DOI: http://dx.doi.org/10.12989/imm.2008.1.4.411

Atomistic simulation and investigation of nanoindentation, contact pressure and nanohardness

Chuin-Shan Chen*, Chien-Kai Wang‡ and Shu-Wei Chang§

Department of Civil Engineering, National Taiwan University, Taipei 10617, Taiwan

(Received October 9, 2008, Accepted November 24, 2008)

Abstract. Atomistic simulation of nanoindentation with spherical indenters was carried out to study dislocation structures, mean contact pressure, and nanohardness of Au and Al thin films. Slip vectors and atomic stresses were used to characterize the dislocation processes. Two different characteristics were found in the induced dislocation structures: wide-spread slip activities in Al, and confined and intact structures in Au. For both samples, the mean contact pressure varied significantly during the early stages of indentation but reached a steady value soon after the first apparent load drop. This indicates that the nanohardness of Al and Au is not affected by the indentation depth for spherical indenters, even at the atomistic scale.

Keywords: nanohardness; contact pressure; contact area; nanoindentation; molecular dynamics; size effects; dislocation.

1. Introduction

The mechanical properties of nanomaterials have received considerable interest lately (Edelstein and Cammarata 1998, Meyers 2006). Due to small intrinsic volumes, materials at the nanoscale often behave differently from their macroscopic counterparts. The resulting mechanical properties at nanoscale serve as a source of inspiration for many novel applications. For example, Liao *et al.* (2005) reported that nanocrystalline silicon carbide films with grain sizes of 5 to 20 nm have hardness values largely exceeding that of the bulk hardness. This property of extreme hardness could have high promise in producing hard protective coatings for cutting tools, computer hard disks, wear resistance applications, etc.

Nanoindentation techniques have often been used to characterize mechanical properties at the nanoscale (Fischer-Cripps 2002). In order to understand detailed deformation and dislocation mechanisms behind nanoindentation testing, researchers have recently resorted to atomistic simulation (Kiely and Houston 1998, Gannepalli and Mallapragada 2002, Liang *et al.* 2003, Lilleodden *et al.* 2003). Kiely and Houston (1998) studied the nanomechanical properties of the (111), (001), and (110) surfaces of gold (Au). An interfacial force microscope was used together with atomistic simulation to quantify the anisotropic variation of the indentation modulus and the

* Corresponding Author, Associate Professor, E-mail: dchen@ntu.edu.tw
‡ Graduate Research Associate
§ Graduate Student

initial yield stress. Gannepalli and Mallapragada (2002) proposed an atomic step mechanism to explain the cause of the observed pyramidal defect structure during Au nanoindentation. The pyramidal defect structure was identified to be responsible for the work-hardening phenomenon. Lilleodden *et al.* (2003) carried out an atomistic study of Au nanoindentation and reported that the elastic anisotropy agrees with the experimental results of Kiely and Houston (1998). They also reported that the calculated mean contact pressure reached a critical value of 22 GPa at which dislocation nucleation occurred. The mean contact pressure then dropped to 12 GPa after nucleation. The mean contact pressure at the fully developed plastic zone equates to the hardness of the material. It is thus of great theoretical and practical interest to study the possible variation of the mean contact pressure and hardness as the indentation depth increases.

The objective of this study is to investigate the possible depth size effects of the mean contact pressure and nanohardness for gold (Au) and aluminum (Al) thin films as well as the consequent dislocation structures and slip mechanisms. To achieve this, the atomistic simulation of nanoindentation with spherical indenters was utilized. The slip vector and atomic stress were then used to quantify dislocation activities in the Au and Al thin films (Zimmerman *et al.* 2001). Finally, the possible depth size effects of the mean contact pressure and nanohardness were studied.

2. Methodology

2.1 Molecular dynamics

Classical molecular dynamics has been widely used to study the mechanical properties of nano-systems (Zhao and Aluru 2008). This methodology was employed to study the desired microstates of atoms subject to indentation and to compute the macroscopic properties resulting from the behavior of a collection of atoms. In classical molecular dynamics, the equations defining the motion of atoms follow trajectories governed by Newtonian dynamics:

$$m_i \ddot{\mathbf{r}}_i = -\frac{\partial \Pi}{\partial \mathbf{r}_i} = \mathbf{f}_i, \qquad i = 1, 2, \ldots, N \tag{1}$$

where m_i is the mass, $\mathbf{r}_i$ is the position vector, and $\mathbf{f}_i$ is the force of an atom i, respectively. Π is the total energy of the mechanical system consisting of the internal atomic potential and external work:

$$\Pi = U + W \tag{2}$$

where U is the internal atomic potential and W is the external work exerted on the system. The internal atomic potential U can be obtained by summing the interatomic potential. For metals, the interatomic potential is often described using the embedded atom method (EAM; Baskes 1992). With EAM, the interatomic potential includes not only the pair potential between two atoms but also the embedded energy induced by the local density of electrons surrounding the atoms of interest. Note that the concept of local density is crucial for the description of metallic bonding. It allows one to account for the dependence of the strength of individual bonds on a local environment. This is especially important for the simulation of surfaces and defects. The energy of an atom i can be described using EAM as:

$$E_i = F(\rho_i) + \frac{1}{2}\sum_{j \neq i}^{N} \phi_{ij}(r_{ij}) \tag{3}$$

$$\rho_i = \sum_{j \neq i}^{N} f(r_{ij}) \tag{4}$$

where $F(\rho_i)$ is the embedded energy, ρ_i is the total electron density of atom i (obtained by summing the neighboring local electron density f), ϕ_{ij} is the pair potential between atoms i and j, and r_{ij} is the distance between atoms i and j.

2.2 Nanoindentation

Nanoindentation using a spherical indenter was implemented to model the nanoindentation experiments. The assembly of atoms with a cubic lattice was used to model the indenter, which provided contact for the surfaces of the metallic thin-film specimens. The force relationship between the atoms of the thin-film sample and the atoms of the indenter characterizes the rigidity of the indenter. The relationship can be described by an indenter-sample interaction potential. In this study, a purely repulsive force relationship given by Gannepalli and Mallapragada (2002) was adopted:

$$F = \varepsilon \left(\frac{r}{\rho}\right)^{-12} \tag{5}$$

where r is the distance from an indenter atom to an atom in the specimen. The parameters $\varepsilon = 25$ meV and $\rho = 3$ Å were used herein. These parameters closely represent the behavior of a rigid indenter.

To obtain equilibrium configurations at various indentation stages, an energy minimization scheme was used. At the equilibrium state, the total force associated with the internal atomic potential and the external work on atom i must equal to zero. Thus, we have:

$$\mathbf{f}_i = -\frac{\partial \Pi}{\partial \mathbf{r}_i} = -\left(\frac{\partial U}{\partial \mathbf{r}_i} + \frac{\partial W}{\partial \mathbf{r}_i}\right) = 0 \tag{6}$$

In Eq. (6), the terms $-\frac{\partial U}{\partial \mathbf{r}_i}$ and $-\frac{\partial W}{\partial \mathbf{r}_i}$ represent the internal force from atomic interactions and the external force from the indenter, respectively. The internal force $\mathbf{f}_i^{\text{int}}$ exerted on atom i can be calculated by taking the derivative of Eq. (5):

$$\mathbf{f}_i^{\text{int}} = -\sum_{j \neq i} \{\phi'_{ij}(r_{ij}) + [F'(\rho_i) + F'(\rho_j)] f'(r_{ij})\} \frac{\mathbf{r}_{ij}}{r_{ij}} \tag{7}$$

where $\mathbf{r}_{ij} = \mathbf{r}_j - \mathbf{r}_i$. The external force exerted on atom i is obtained by simply summing the repulsive force contributions from Eq. (5).

During the energy minimization process, the total force on each atom will not be zero initially. The unbalanced force serves as the driving gradient to move the state approaching equilibrium. In this study, each new stable equilibrium configuration was obtained using the Polak-Ribiere variation of the conjugate gradient method (Press *et al.* 2002).

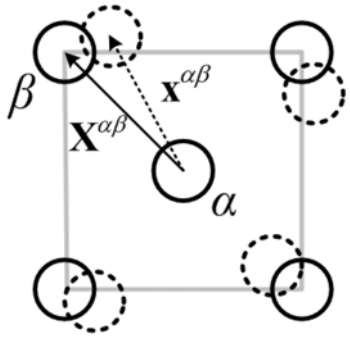

Fig. 1 Illustration of the slip vector

2.3 Slip vector and atomic stress

To quantitatively describe the dislocation processes from the atomistic simulation, the slip vector given by Zimmerman *et al.* (2001) was adopted. The slip vector of an atom, α, as illustrated in Fig. 1 is defined as:

$$\mathbf{s}^{\alpha} = -\frac{1}{n_s}\sum_{\beta}(\mathbf{r}^{\alpha\beta} - \mathbf{R}^{\alpha\beta}) \tag{8}$$

where the index β goes through the nearest neighbors of atom α, n_s is the number of slipped neighbors of atom α, and $\mathbf{r}^{\alpha\beta}$ and $\mathbf{R}^{\alpha\beta}$ are the vector differences between the atoms α and β in the current and reference states, respectively. The initial state prior to indentation is often used as the reference state. The slip vector closely represents the Burger vector and can be used to characterize the slip of adjacent atomic planes.

Another useful quantity for characterizing the influence of dislocations is atomic stress. In molecular dynamics simulations, the Virial stress definition is often utilized to calculate the stress of the deformed configuration (Cormier *et al.* 2001). The Virial stress tensor for static problems is:

$$\boldsymbol{\sigma}_{\alpha\beta}^{Virial} = \frac{1}{2\boldsymbol{\Omega}}\sum_{i\neq 1}^{N}\sum_{j\neq i}^{N}\left(-\frac{\partial U}{\partial r_{ij}}\right)\frac{r_{ij}^{\alpha}\, r_{ij}^{\beta}}{|\mathbf{r}_{ij}|} \tag{9}$$

where α and β denote the Cartesian components, and N is the number of atoms contained in the averaging volume $\boldsymbol{\Omega}$.

Strictly speaking, stress can only be definded in a medium for which the densities of mass, momentum and energy are continuously distributed. Care must be taken when using the stress to interpret internal responses of atoms whose motion is discontinuous in nature. Thus, an acceptable variability and defining dimension need to be introduced to justify its usage for any discrete simulation such as molecular dynamics simulation used herein (Fung 1993, Rojek and Onate 2008). In this study, the atomic volume was used to represent the average volume $\boldsymbol{\Omega}$. This treatment may be sufficient to characterize the qualitative influence of dislocations.

3. Nanohardness

The mean contact pressure, obtained by dividing the indenter load by the projected contact area,

characterizes the material support beneath the indenter. When determined at the fully developed plastic zone, the mean contact pressure equates to the hardness of the material. In conventional indentation testing, the hardness H is determined from the peak of the indentation load ($P_{\max}$) divided by the residual contact area (A_c) after the removal of the load, i.e.:

$$H = \frac{P_{\max}}{A_c} \tag{10}$$

However, it is very difficult to directly measure the residual contact area of the specimen using the indentation apparatus at the nanoscale. To overcome this difficulty, nanoindentation testing often relies on the indirect measurement of the contact area through the penetration depth and known geometry of indenters. Thus, nanoindentation is also known as depth sensing indentation (Fischer-Cripps 2002, Oliver and Pharr 1992).

There are many semi-analytical and empirical relations for determining the contact area function; see Fischer-Cripps (2002) for detailed descriptions of various relations and their corresponding rationales. For spherical indenters, Herbert *et al.* (2001) proposed a simple model to determine the contact area using the contact depth, h_c:

$$A_c^H = \pi(2h_c R - h_c^2) \tag{11}$$

where R is the indenter radius.

In nanoindentation testing, h_c can be obtained indirectly from elastic unloading, i.e.:

$$h_c = h_{\max} - \varepsilon \frac{P_{\max}}{S} \tag{12}$$

where $h_{\max}$ is the maximum penetration depth, ε is the intercept correct term, and S is the stiffness during elastic unloading. The intercept correct term ε depends on the geometry of the indenters. For example, $\varepsilon = 0.72$ for a conical indenter, $\varepsilon = 0.75$ for a spherical indenter, and $\varepsilon = 1.0$ for a flat punch.

In atomistic modeling of nanoindentation, the contact area A_c can be obtained by triangulating the projected atoms as illustrated in Fig. 2. Moreover, the contact depth h_c can also be directly

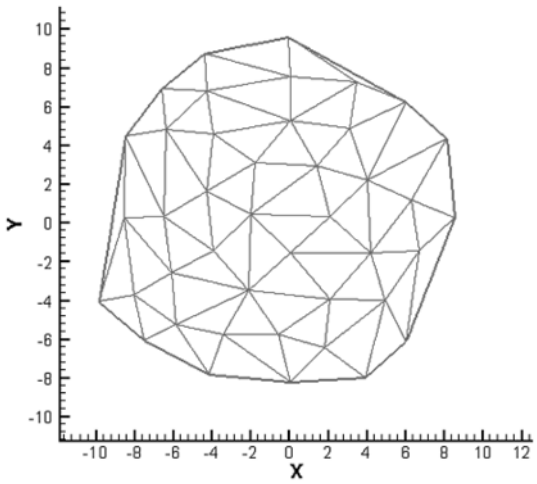

Fig. 2 Projected contact area obtained from triangulation

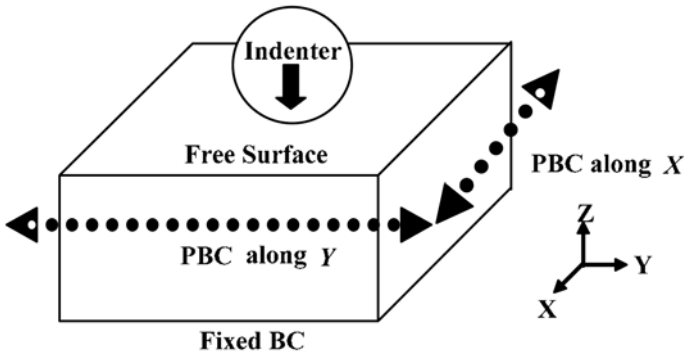

Fig. 3 Schematic of indentation simulation box and boundary conditions

determined from simulations by looping through the atoms that come in contact with the indenter. In the following, A_c^H and A_c^T denote the projected contact areas obtained from Eq. (11) and the triangulation of the projected atoms, respectively.

4. Results and discussion

The atomistic model consisted of the (001) surface of a face-centered cubic (FCC) crystalline thin film of Al and Au atoms and a spherical indenter. The thin film model was configured using a box of dimension 320 Å × 276 Å × 195 Å (containing approximately one million atoms). The atoms in this box were oriented so that the [100], [010], and [001] crystallographic directions were parallel to the X, Y, and Z Cartesian coordinates, respectively. Periodical boundary conditions were imposed along the X and Y directions and fixed boundary conditions were exerted on the bottom of the samples to represent thin film samples (Fig. 3).

4.1 Dislocation activities in nanoindentation

Fig. 4 shows the simulated curves for the indenting load versus indentation depth. The indenting load was obtained from summing the total *Z*-direction forces exerted on the indenter atoms. The indentation depth was taken as the indenter displacement.

The inflection points in Fig. 4 indicate the major dislocation events during nanoindentation. Throughout the simulation, transitions of the dislocation defect structures accompanying load drop events were observed, similar to those reported in Liang *et al.* (2003). All dislocations took place on the preferred slip planes {111}, consistent with those predicted by the dislocation theory for an FCC crystalline solid (Hirth and Lothe 1982). For the Al sample, the first apparent load drop appeared at an indentation depth of 10.1 Å. Before this depth, there were a few defects in the form of hillocks that resulted in minor load drops. At a depth of 10.1 Å, the dissociation of a V-shaped loop along the {111} planes was observed (Fig. 5). The nucleation of dislocation structures also induced stress re-distribution. Figs. 6 and 7 show the atomic shear stresses depicted at an indentation depth of 10.1 Å and 10.2 Å, respectively. Stress evolution along the dislocation loop was clearly observed.

The load versus depth curve for Al rose quasi-elastically between a depth of 10.1 Å and 13.1 Å as shown in Fig. 4, which can be attributed to equilibrium between the external stress applied by the

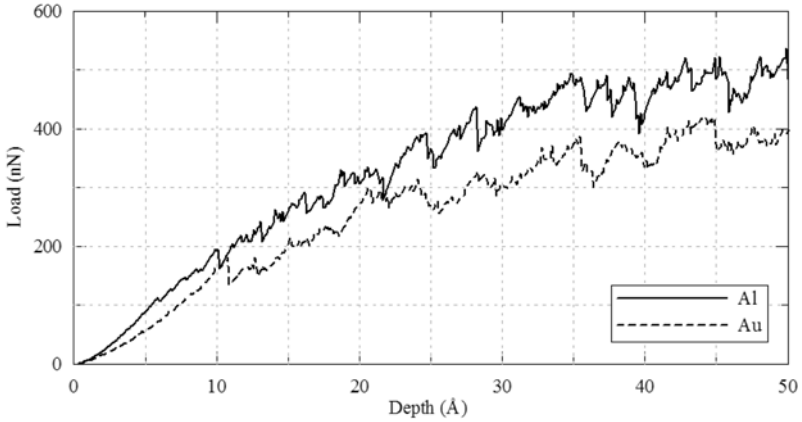

Fig. 4 Load versus depth for the indentation simulation

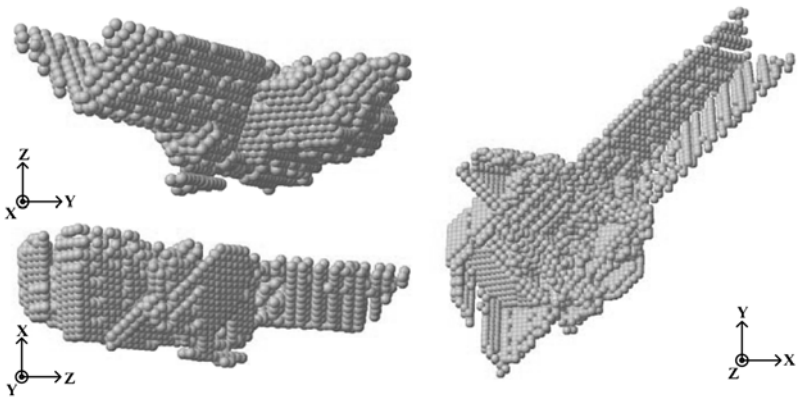

Fig. 5 Dislocation structures at an indentation depth of 10.1 Å for Al

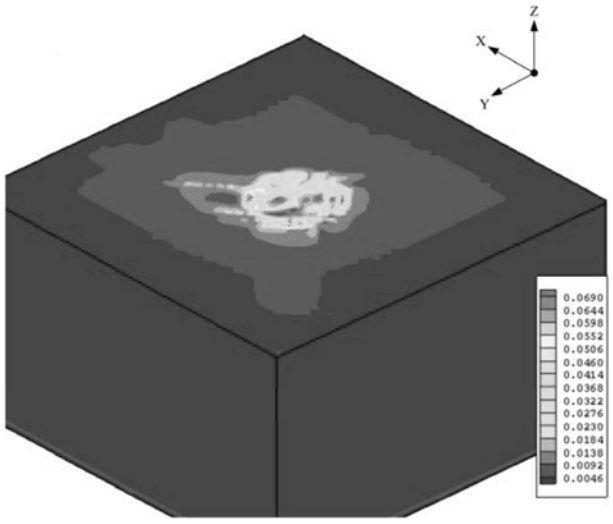

Fig. 6 Atomic shear stress contour at an indentation depth of 10.1 Å for Al

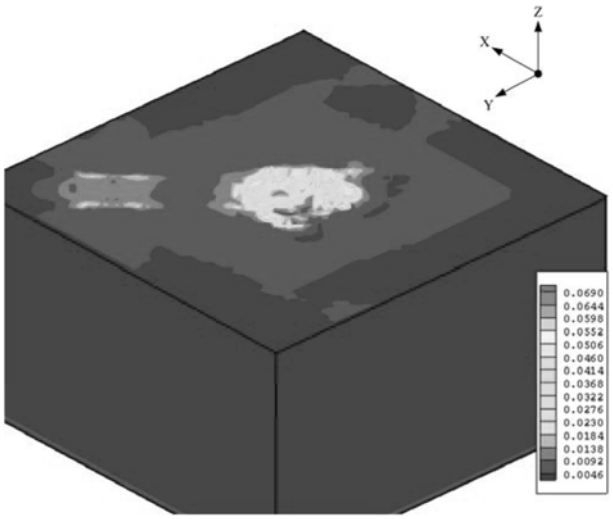

Fig. 7 Atomic shear stress contour at an indentation depth of 10.2 Å for Al

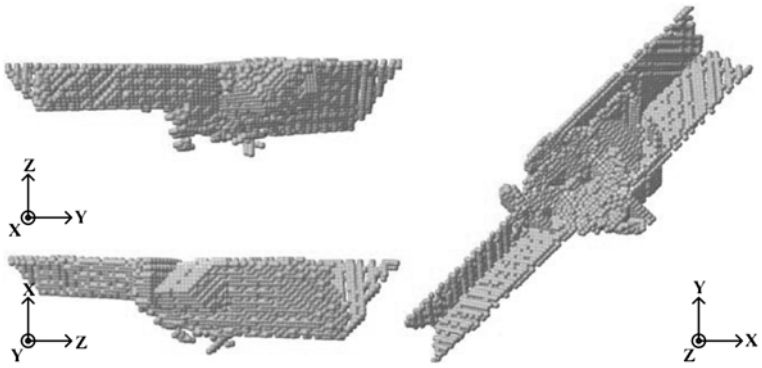

Fig. 8 Dislocation structures at an indentation depth of 13.1 Å for Al

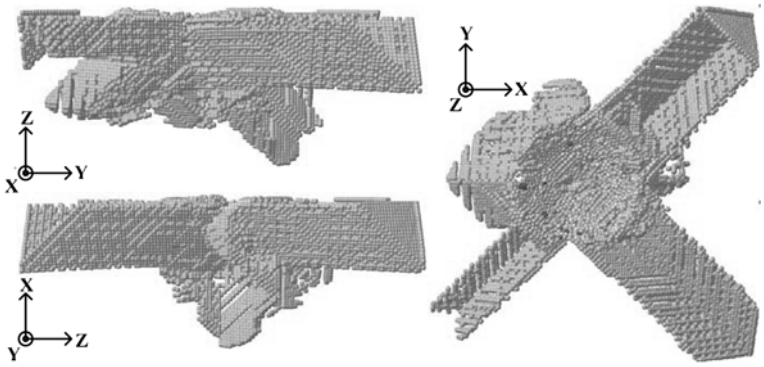

Fig. 9 Dislocation structures at an indentation depth of 21.1 Å for Al

indenter and the back stress induced by the dislocation loops. At a depth of 13.1 Å, another V-shaped loop occurred in the opposite direction, as shown in Fig. 8. The two dislocation loops glided

along the $[1\bar{1}0]$ and $[\bar{1}\bar{1}0]$ directions and left traces behind them on the two sets of the slip planes $[111]$ and $[\bar{1}\bar{1}1]$. The nucleation of these dislocation loops manifested itself in the load versus depth curve and resulted in a considerable load drop. After a depth of 13.1 Å, the curve rose again until another load drop occurred at 21.1 Å. At a depth of 21.1 Å, a new dislocation loop, as shown in Fig. 9, nucleated and glided along the $1\bar{1}0$ direction.

For the Au sample, there were also several load drops corresponding to the generation of defect structures. The first apparent load drop occurred at an indentation depth of 10.8 Å. Compared with the defect structure at the first apparent load drop of Al, the dislocation structure of Au shown in Fig. 10 did not contain wide-spreading V-shaped loops. On the contrary, the dislocation structures were relatively intact as Au indentation continued (Figs. 11 and 12) and only some hillock defects were observed.

The difference between induced dislocation structures in Al and Au is mainly caused by cross slip activities. Cross slip is a process of moving screw dislocations from one {111} plane to another. It occurs more easily in metals with higher stacking fault energy (Hull and Bacon 2001). The stacking fault energy for Al is about five times larger than that for Au (Cousland 1970). Consequently, the cross slip events are more likely to occur in Al and result in a wider spread of slip activities in Al.

Fig. 10 Dislocation structures at an indentation depth of 10.8 Å for Au

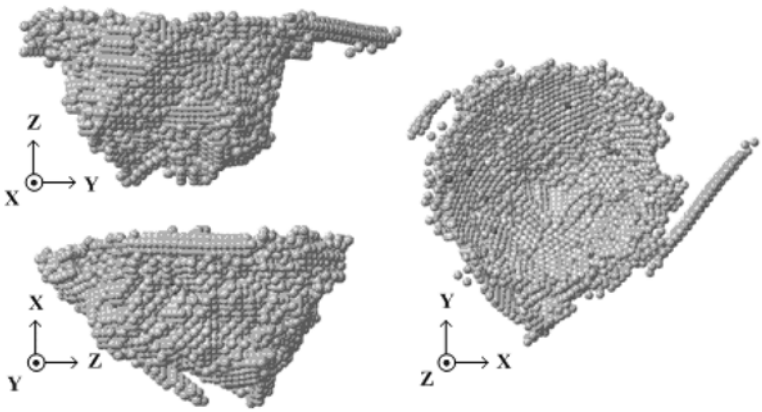

Fig. 11 Dislocation structures at an indentation depth of 20.2 Å for Au

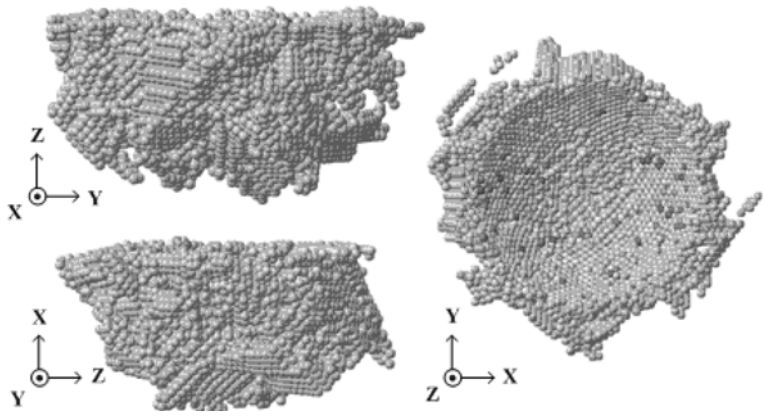

Fig. 12 Dislocation structures at an indentation depth of 26.8 Å for Au

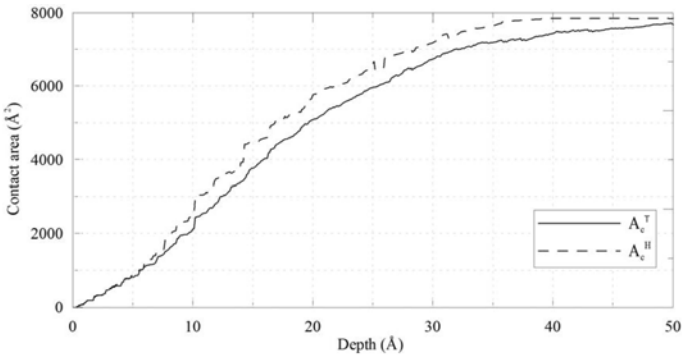

Fig. 13 Contact area vs. depth for the Al indentation simulation

4.2 Indentation depth effect on the mean contact pressure and nanohardness

The mean contact pressure can be readily evaluated from atomistic calculations. The contact areas at each indentation depth were obtained directly by computing the projected convex area of the contact atoms. Figs. 13 and 14 plot the contact area versus depth for the Al and Au simulation indentations with maximum depths of 50 Å. The curves go up in a ladder-like fashion as the indentation depth increases. This behavior reflects the underlying discrete nature of atomistic modeling. Contact areas obtained from Eq. (11) are also plotted in Figs. 13 and 14. Contact areas obtained directly from triangulation and from the semi-analytical relation given in Eq. (11) showed good agreement before the occurrence of dislocation activities. However, deviations between the two were observed as the dislocations began to occur. Moreover, the deviation was observed before the first apparent load drop in Al (~6 Å vs. 10.1 Å), attributed to the occurrence of hillocks prior to the load drop. For Au, the deviation coincided with the first apparent load drop.

It is of great theoretical and practical interest to study depth size effects on the mean contact pressure and nanohardness through atomistic simulation. Fig. 15 plots the calculated mean contact pressure of Al and Au vs. the indentation depth. Two significant results were observed. Firstly, a general trend was observed: the computed values of mean contact pressure varied significantly at the early stage of indentation but reached a steady value soon after the first apparent drop. As the

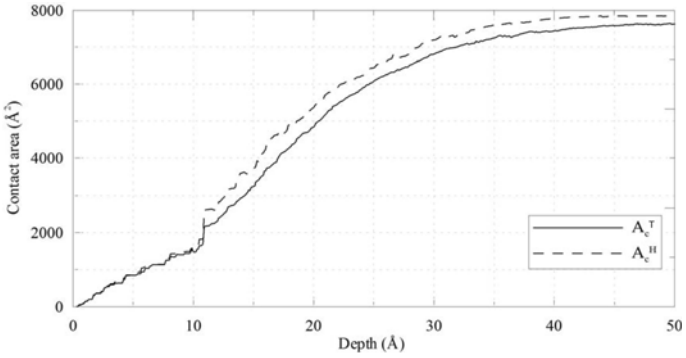

Fig. 14 Contact area vs. depth for the Au indentation simulation

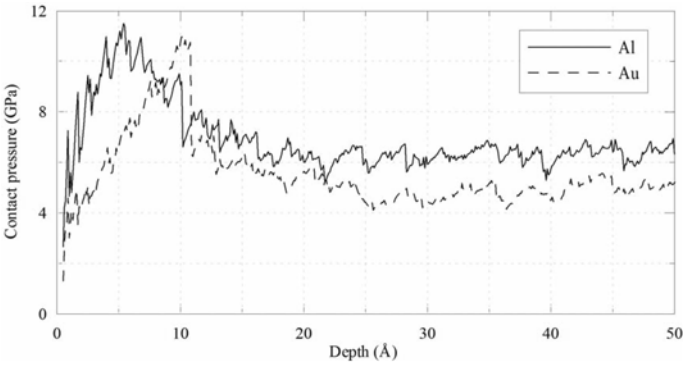

Fig. 15 Mean contact pressure vs. depth for the Al and Au indentation simulations

mean contact pressure at the fully developed plastic zone equates to the hardness of materials, this steady value can be interpreted as the nanohardness of materials. This observation indicates that the nanohardness of Al and Au is not affected by the indentation depth for spherical indenters, even at the atomistic scale. It also implies that dislocation activities beneath the spherical indenter are fully developed. Secondly, the peak of the mean contact pressure for Al occurred before the first apparent load drop. In contrast, this peak coincided with the first apparent load drop for Au. This can be explained by the occurrence of hillocks prior to the load drop in Al. Although such dislocation activities were not significant enough to trigger a major load drop, they signified plasticity incipiency. The incipiency of plasticity thus determines the peak of the mean contact pressure.

5. Conclusions

Atomistic simulation of nanoindentation using spherical indenters was carried out to study dislocation structures, mean contact pressure, and nanohardness of Au and Al thin films. V-shaped dislocation loops progressing away from the indenter were observed in Al while an intact dislocation structure was observed in Au. The difference between induced dislocation structures in Al and Au is mainly governed by cross slip activities and stacking fault energy. For both samples, the mean contact pressure varied significantly at the early stage of indentation but reached a steady

value soon after the first apparent load drop. This indicates that the nanohardness of Al and Au is not affected by the indentation depth for spherical indenters, even at the atomistic scale. Finally, the incipiency of plasticity, whether it is capable of triggering a major load drop, determines the peak of the mean contact pressure.

Acknowledgements

This research was supported by the National Science Council in Taiwan under the award no. 95-2218-E-002-029. We are also grateful to the National Center for High-Performance Computing and National Taiwan University for providing the computational resources required for this study.

References

Baskes, M. I. (1992), "Modified embedded-atom potentials for cubic materials and impurities", *Physical Review B*, **46**, 2727-2742.

Cormier, J., Rickman, J. M. and Delph, T. J. (2001), "Stress calculation in atomistic simulations of perfect and imperfect solids", *J. Appl. Phy.*, **89**(1), 99-104.

Cousland, S. McK. (1970), "Cottrell-Stokes ratios and stacking fault energies", *Phys. Stat. Sol.* **37**, 159.

Edelstein, A. S. and Cammarata, R. C. (1996), *Nanomaterials: Synthesis, Properties and Application*, Institute of Physics Publishing.

Fischer-Cripps, A. C. (2002), *Nanoindentation*, Springer.

Fung, Y. C. (1993), *First Course in Continuum Mechanics*, 3rd Edition, Prentice Hall.

Gannepalli, A., Mallapragada, S.K. (2002), "Atomistic studies of defect nucleation during nanoindentation of Au (001)", *Physical Review B*, **66**, 104103.

Herbert, E. G., Pharr, G. M., Oliver, W. C., Lucas, B. N. and Hay, J. L. (2001), "On the measurement of stress-strain curves by spherical indentation", *Thin Solid Films,* **398-399**, 331-335.

Hirth, J. P. and Lothe, J. (1982), *Theory of Dislocations*, Wiley.

Kiely, J. D. and Houston, J. E. (1998), "Nanomechanical properties of Au (111), (001), and (110) surfaces", *Physical Review B*, **57**, 12588.

Liang, H. Y., Woo, C. H., Huang, H., Ngan, A. H. W. and Yu, T. X. (2003), "Dislocation nucleation in the initial stage during nanoindentation", *Philosophical Mag.*, **83**(31), 3609-3622.

Liao, F., Girshick, S. L., Mook, W. M., Gerberich, W. W. and Zachariah, M. R. (2005), "Superhard nanocrystalline silicon carbide films", *Appl. Phys. Lett.* **86**, 171913.

Lilleodden, E. T., Zimmerman, J. A., Foiles, S. M. and Nix, W. D. (2003), "Atomistic simulations of elastic deformation and dislocation nucleation during nanoindentation", *J. Mech. Phys. Solids*, **51**(5), 901-920.

Meyers, M. A., Mishra, A. and Benson D. J. (2006), "Mechanical properties of nanocrystalline materials", *Progress in Materials Science*, **51**(4), 427-556.

Oliver, W. C. and Pharr, G. M. (1992). "Improved technique for determining hardness and elastic modulus using load and displacement sensing indentation experiments", *J. Mater. Res.*, **7**(6), 1564-1580.

Press, W. H., Teukolsky, S. A., Vetterling, W. T. and Flannery, B. P. (2007), *Numerical Recipes 3rd Edition: The Art of Scientific Computing*, Third Edition Cambridge University Press.

Rojek, J. and Onate, E. (2008), "Multiscale analysis using a coupled discrete/finite element model", *Interaction and Multiscale Mechanics, An Int. J.*, **1**(1), 1-31.

Zhao, H. and Aluru, N. R. (2008), "Molecular dynamics simulation of bulk silicon under strain", *Interaction and Multiscale Mechanics, An Int. J.*, **1**(2), 303-315.

Zimmerman, J. A., Kelchner, C. L., Klein, P. A., Hamilton, J. C. and Foiles, S. M. (2001), "Surface step effects on nanoindentation", *J. Appl. Phy.*, **89**(1), 99-104.